# A multi-scale comparison of modeled and observed seasonal methane emissions in northern wetlands

Xiyan Xu[1], William J. Riley[1], Charles D. Koven[1], Dave P. Billesbach[2], Rachel Y.-W. Chang[3, 4], Róisín Commane[3], Eugénie S. Euskirchen[5], Sean Hartery[4], Yoshinobu Harazono[6, 7], Hiroki Iwata[6, 8], Kyle C. McDonald[9, 10], Charles E. Miller[10], Walter C. Oechel[11, 12], Benjamin Poulter[13], Naama Raz-Yaseef[1], Colm Sweeney[14, 15], Margaret Torn[1, 16], Steven C. Wofsy[3], Zhen Zhang[15, 17] , Donatella Zona[11, 18]

[1]Earth Sciences Division, Lawrence Berkeley National Laboratory, Berkeley, California, USA;
[2]Biological System Engineering Department, University of Nebraska, Lincoln, Nebraska;
[3]School of Engineering and Applied Sciences, Harvard University, Cambridge, Massachusetts, USA;
[4]Department of Physics and Atmospheric Science, Dalhousie University, Halifax, Nova Scotia, Canada;
[5]Institute of Arctic Biology, University of Alaska Fairbanks, Fairbanks, Alaska, USA;
[6]International Arctic Research Center, University of Alaska Fairbanks, Fairbanks, Alaska, USA;
[7]Graduate School of Life and Environmental Sciences, Osaka Prefecture University, Sakai, Osaka, Japan;
[8]Department of Environmental Sciences, Faculty of Science, Shinshu University, Matsumoto, Nagano, Japan;
[9]Department of Earth and Atmospheric Sciences, CUNY Environmental Crossroads Initiative and NOAA-CREST Institute, The City College of New York, City University of New York, New York
[10]Jet Propulsion Laboratory, California Institute of Technology, Pasadena, California, USA;
[11]Global Change Research Group, Department of Biology, San Diego State University, San Diego, California, USA;
[12]Department of Environment, Earth and Ecosystems, The Open University, Milton Keynes, U. K. MK7 6AA;
[13]Department of Ecology, Montana State University, Bozeman, MT 59717, USA
[14]Cooperative Institute for Research in Environmental Sciences, University of Colorado, Boulder, CO, 80304
[15]NOAA Earth System Research Laboratory, Global Monitoring Division, Boulder, CO, USA
[16]Energy and Resources Group, University of California-Berkeley, Berkeley, California, USA;
[17]Swiss Federal Research Institute WSL, Birmensdorf 8059, Switzerland
[18]Department of Animal and Plant Sciences, University of Sheffield, Sheffield S102TN, United Kingdom.

Correspondence to : Xiyan Xu (xxu@lbl.gov)

**Abstract:**
Wetlands are the largest global natural methane ($CH_4$) source, and emissions between 50°N and 70°N latitude contribute 10-30% to this source. Predictive capability of land models for northern wetland $CH_4$ emissions is still low due to limited site measurements, strong spatial and temporal variability in emissions, and complex hydrological and biogeochemical dynamics. To explore this issue, we compare wetland $CH_4$ emission predictions from the Community Land Model 4.5 (CLM4.5-BGC) with site to regional scale observations. A comparison of the $CH_4$ fluxes with eddy flux data highlighted needed changes to the model's estimate of aerenchyma area, which we implemented and tested. The model modification substantially reduced biases in $CH_4$ emissions when compared with CarbonTracker $CH_4$ predictions. CLM4.5 $CH_4$ emission predictions agree well with growing season (May-September) CarbonTracker Alaskan regional-level $CH_4$ predictions and site-level observations. However, CLM4.5 underestimated $CH_4$ emissions in the cold season (October-April). The monthly atmospheric $CH_4$ mole fraction enhancements due to wetland emissions are also assessed using the WRF-STILT Lagrangian transport model coupled with daily emissions from CLM4.5 and compared with aircraft $CH_4$ mole fraction measurements from the Carbon in Arctic Reservoirs Vulnerability Experiment (CARVE) campaign. Both the tower and aircraft analyses confirm the underestimate of cold season $CH_4$ emissions by CLM4.5. The greatest uncertainties in predicting the seasonal $CH_4$ cycle are from the wetland extent, cold season $CH_4$ production and $CH_4$ transport processes. We recommend more cold-season experimental studies in high latitude systems, which could improve understanding and parameterization of ecosystem structure and function during this period. Predicted $CH_4$ emissions remain uncertain, but we show here that benchmarking against observations across spatial scales can inform model structural and parameter improvements.

## 1 Introduction

Natural wetlands are the largest natural methane ($CH_4$) source, contributing up to 34% of global $CH_4$ emissions (Kirschke et al., 2013). Between 1980 and 2009, estimated global annual $CH_4$ emissions from wetlands varied from 115 to 231 Tg $CH_4$ in top-down atmospheric inversion models and 169 to 284 Tg $CH_4$ in bottom-up process-based land models (Kirschke et al., 2013). Peat-rich bogs and fens lying between 50°N and 70°N constitute about half of the global wetland area, and release 10-30% of the total wetland $CH_4$ (Wania et al., 2010; Zhuang et al., 2004; Bergamaschi et al., 2009; Riley et al., 2011). Much of the northern wetland area is in the permafrost zone, which stores 1035±150 Pg soil organic carbon for the 0-3m soil depth (Hugelius et al., 2014). When permafrost soils thaw, $CH_4$ is produced under anaerobic conditions by methanogenic archaea. Once $CH_4$ is produced, it can be oxidized by methanotrophic archaea. $CH_4$ surface emissions occur through several transport pathways: aqueous and gaseous diffusion, ebullition, and aerenchyma diffusion and advection. At any point in the soil, the $CH_4$ concentration is governed by the balance between $CH_4$ production in anoxic zones, $CH_4$ consumption in oxic zones, transport, and atmospheric $CH_4$ diffusion at the soil-atmosphere interface.

Many interacting factors (e.g., temperature, thaw depth, soil moisture, depth of the water table, vegetation type) affect $CH_4$ production and emission. $CH_4$ production has a positive response to temperature increase (Van Hulzen et al., 1999; van Winden et al., 2012; Hommeltenberg et al., 2014) and laboratory incubations of soil samples from the active layer show that large variability of $Q_{10}$ values for $CH_4$ production (1.5 to 28, Segers et al., 1998) is related to site-specific peatland type and organic matter quality (Lupascu et al., 2012). $CH_4$ emissions also show positive temperature dependence above freezing. The temperature dependence of surface $CH_4$ emission is much stronger than that of respiration and photosynthesis, which indicates increases in both $CH_4$ emissions and the ratio of $CH_4$ to $CO_2$ emissions with seasonal increases in temperature (Yvon-Durocher et al., 2014). The positive temperature dependence of $CH_4$ emissions may only be valid when $CH_4$ oxidation is less sensitive to temperature (van Winden et al., 2012). The $Q_{10}$ value for $CH_4$ oxidation was reported to be 1.4 to 2.1 in northern peat soils (Dunfield et al., 1993). Strong oxidation temperature sensitivity can lead to decreased $CH_4$ surface emissions with rising temperature (Wang et al., 2014). The positive dependence of $CH_4$ emissions on soil temperature can be most significant in areas with sufficient soil moisture or a shallow water table (Roulet et al., 1992; Moosavi et al., 1996; Wickland et al., 1999). The dependency of $CH_4$ emissions on temperature can vanish at high temperature and low water table (Hommeltenberg et al., 2014). At low water table levels, large $CH_4$ oxidation can mask the $CH_4$ production temperature sensitivity in the net emissions. $CH_4$ production under sub-zero temperatures was reported in incubation experiments (Clein and Schimel, 1995; Brouchkov et al., 2003), however, the mechanisms that regulate $CH_4$ production under cold temperatures have not been clarified.

Soil water content exerts strong control on $CH_4$ emissions by affecting belowground carbon decomposition and root growth (Iversen et al., 2015). A lowered water table typically reduces $CH_4$ production and emission, because of a higher aerobic to anaerobic respiration ratio in the soil column and $CH_4$ oxidation during diffusive

transport through the oxygen-rich surface layer (Whalen and Reeburgh, 1990). If $CH_4$ produced in anoxic zones (e.g., below the water table) is transported to the atmosphere through aerenchyma, the impact of methanotrophy on net $CH_4$ emissions is diminished (Bartlett et al., 1992; Torn and Chapin, 1993; King et al., 1998; Juutinen et al., 2003; McEwing et al., 2015). The reduced methanotrophic impacts vary with vascular species cover and root density and are more common in tall vegetation, because taller plants have more extensive root systems that enable more methanogenesis and pore water $CH_4$ to escape to the atmosphere (van Fischer et al., 2010). The correlation between water table depth and $CH_4$ emission can be very weak if the water table drops in an already oxic surface layer (Sturtevant et al., 2012).

The seasonal cycle of $CH_4$ emissions and their physical controls are strongly controlled by the freeze-thaw cycle in northern wetlands, and its regulation of wetland extent. The northern wetland area retrieved from the 19- and 37-GHz passive microwave Special Sensor Microwave/Image (SSM/I) brightness temperature database shows that maximum inundation is usually observed during July, August, and September in north America (48°N-68°N) and between June and September in northern Eurasia (Mialon et al., 2005). The inundation dynamics retrieved from SSM/I and ISCCP observations, ERS scatterometer responses, and AVHRR visible and near-infrared reflectance also show that maximum inundation occurs in July and August in northern boreal regions (55°N-70°N) (Prigent et al., 2007). The inferred wetland extent increases rapidly during the spring thaw period and shrinks again during the fall freeze period; though it is unclear at large scales how much of this seasonal cycle is due to changes in the areal fraction of land in which water ponds at the surface versus changes in the phase of that water. The interannual variability of high-latitude summer wetland extent is very small. Larger interannual variability during the intermediate seasons arises from the large variability of the timing and extent of snowmelt and accumulation (Mialon et al., 2005). For boreal bogs north to 50°N, the variation in wetland area contributed about 30% to the annual emissions and can explain the interannual variation in regional $CH_4$ emissions (Ringeval et al., 2010).

Site measurements have shown great variability in seasonal $CH_4$ emissions (Wilson et al., 1989; Mastepanov et al., 2008; 2013; Zona et al., 2016). In the late fall to winter, the surface water or shallow peat zone are frozen, and $CH_4$ produced below the frozen layer can be trapped. Only a small portion of the trapped $CH_4$ is oxidized because of low oxygen concentrations below the frozen layer (Mastepanov et al., 2008). Observed $CH_4$ emissions during spring thaw are highly variable and contribute substantially to total annual emissions. $CH_4$ fluxes during the spring thaw period contributed 11% to the annual budget over an aapa mire in Finnish Lapland (Hargreaves et al., 2001). The emission amounts can be 24% of the total annual emissions during the spring period after snowmelt next to an open pool in Caribou Bog, Maine, while the proportion can be as high as 77% in the adjacent upland area (Comas et al., 2008). In the non-inundated upland tundra, the cold season (September to May) emissions account for more than 50% of the annual $CH_4$ emissions (Zona et al., 2016). Although wetlands can contribute a large proportion of annual $CH_4$ emissions during the cold season, the seasonal peak of $CH_4$ emissions is usually observed in the summer (Pickett-Heaps et al., 2011; Zona et al., 2016). A transport model combined with flight measurements showed the peak $CH_4$ emission to be in July-August in the Hudson Bay Lowlands (Pickett-Heaps et al., 2011).

Although the recorded emission pulses during spring thaw and late fall (Song et al., 2012; Tokida et al., 2007; Rinne et al., 2007; Mastepanov et al., 2008; 2013) may be more localized and of minor importance to annual emissions (Chang et al., 2014; Rinne et al., 2007), the pulses indicates the complexity and heterogeneity in the seasonal $CH_4$ cycle.

Many modeling studies have shown that there is large uncertainty in predictions of spatial patterns of $CH_4$ emissions from natural wetlands at the regional and global scales (Melton et al., 2013; Bohn et al., 2015). This uncertainty can be roughly split into poor knowledge of water table and soil moisture dynamics versus poor knowledge of $CH_4$ fluxes per unit area of land with a given water table depth or soil moisture state; both contribute substantially to the overall uncertainty. One approach to reducing this overall uncertainty is to focus on the seasonal cycles of $CH_4$ emissions at the site scale (where inundation dynamics can be more easily constrained) versus at larger scales to ask whether model predictions and errors are consistent across these scales. The temporal dynamics of $CH_4$ emissions over the season cannot be ignored when calculating long-term $CH_4$ budgets (Morin et al., 2014). To investigate the seasonal cycle of $CH_4$ emissions in northern wetlands and the underlying processes in a climate model context, we evaluated and modified the $CH_4$ biogeochemistry module in the Community Land Model (CLM 4.5). Seasonal cycles of $CH_4$ emissions in Alaskan wetlands are analyzed based on the modified model predictions, $CH_4$ emission measurements at high-latitude sites, CarbonTracker $CH_4$ emission estimates, and atmospheric inversion estimates of surface $CH_4$ emissions from data collected in the Carbon in Arctic Reservoirs Vulnerability Experiment (CARVE). The models and data are described in section 2. Multi-scale comparison results and discussions are given in section 3, and concluding remarks in section 4.

## 2 Data and Methods

### 2.1 Models description

#### 2.1.1 $CH_4$ model in CLM4.5-BGC

The $CH_4$ biogeochemistry model used here (CLM4Me; Riley et al. (2011)) has been coupled to the revised land model CLM4.5, which includes numerous changes to vegetation, soil biogeochemistry, and hydrology from the CLM4.0 in which CLM4Me was originally developed. CLM4Me includes representation of $CH_4$ production, oxidation, and transport through the soil column. Transport includes multiple pathways: aerenchyma transport, ebullition, and aqueous and gaseous diffusion. Aerenchyma is the most efficient pathway for gas exchange between the soil and atmosphere in wetlands or aquatic environments, through which atmosphere $O_2$ is supplied to roots and the rhizosphere while $CH_4$ is removed from the soil to shoots and the atmosphere. In CLM4Me, aerenchyma transport ($A$) is parameterized as gaseous diffusion in response to a concentration gradient between the soil layer ($z$) and the atmosphere ($a$) as:

$$A = \frac{C(z) - C_a}{\frac{r_L z}{Dp T \rho_r} + r_a} \quad , \qquad (1)$$

where $D$ ($m^2\ s^{-1}$) is the free-air gas diffusion coefficient, $C(z)$ (mol $m^{-3}$) is the gaseous concentration at depth z, dimensionless $r_L$ is the ratio of total root length to root depth, $p$ (-) is tiller porosity; $T$ ($m^2\ m^{-2}$) is specific aerenchyma area, $r_a$ (s $m^{-1}$) is the aerodynamic resistance between the surface and the atmospheric reference height, and $r_r$ (-) is the root mass fraction in the soil layer. The aerenchyma area $T$ is seasonally varying with phenology S (described below):

$$T = \frac{f_N N_a S}{0.22} \pi R^2 , \quad (2)$$

where $N_a$ (gC $m^{-2}$) is annual net primary production(NPP), $R$ ($2.9 \times 10^{-3}$ m) is the aerenchyma radius, $f_N$ is the belowground fraction of current NPP, and the factor 0.22 (gC) is the mass of C per tiller. The dimensionless term $S$ is included in CLM4Me to capture seasonal cycles of aerenchymous tissues. In the absence of data on phenology of aerenchyma, $S$ was originally taken as the leaf area index (LAI).

The default method for calculating inundation fraction ($F_{def}$) remains the same as described in Riley et al. (2011), which applied a simple inversion model to represent the spatial inundation:

$$F_{def} = p_1 e^{-z_w/p_2} + p_3 Q_r , \quad (3)$$

The three parameters ($p_1, p_2, p_3$) are optimized with the inundation map by Prigent et al. (2007). $z_w$ is simulated water table depth (m) and $Q_r$ is surface runoff (mm $s^{-1}$). We also applied an estimate of inundation fraction $F_{S+G}$ ( Poulter et al., In Review) derived from seasonal cycle of inundation fraction from the Surface WAter Microwave Product Series Version 2.0 (SWAMPS, Schroeder et al., 2015) developed at the NASA Jet Propulsion Laboratory with the Global Lakes and Wetlands Dataset (GLWD, Lehner and Doll, 2004) to discuss the potential uncertainties in $CH_4$ emissions caused by wetland area.

Our model is driven by half-degree CRUNCEP V5 6-Hourly Atmospheric Forcing dataset (1901-2013) (http://dods.extra.cea.fr/data/p529viov/cruncep/readme.htm). Monthly wetland $CH_4$ emissions are simulated between the year 2000 and 2012 during which $F_{S+G}$ is available. The monthly $CH_4$ emissions in half-degree resolution are regrided to 1°×1° and averaged longitudinally to compare with CarbonTracker predicted $CH_4$ fluxes. Daily wetland $CH_4$ emissions are simulated for year 2012 and 2013 to calculate the atmospheric enhancements of $CH_4$ due to modeled surface emissions.

### 2.1.2 WRF-STILT modeling of $CH_4$ transport

We simulate the atmospheric $CH_4$ mole fraction enhancements due to wetland emissions by combining the CLM4.5 predicted daily surface emissions with the land surface influences ("footprint") calculated by the Weather Research and Forecasting-Stochastic Time-Inverted Lagrangian Transport (WRF-STILT) model (Henderson et al.; 2015). WRF-STILT estimates the upwind surface influence along the flight track of the CARVE aircraft by releasing 500 particles at the point of flight measurement and allowing them to stochastically disperse in reverse time over 10 days (Henderson et al., 2015). The resolution of the resulting footprint sensitivity used in this study is 0.5 °×0.5°, covering 30-90°N, circumpolar. However, we assume that $CH_4$ transported from areas outside of Alaska are most likely mixed thoroughly in the atmosphere before they reach Alaska, and therefore only contribute to the background abundance of $CH_4$.

## 2.2 Measurements of $CH_4$

### 2.2.1 Site-Scale Observations

We compare CLM4.5 $CH_4$ emission predictions with data obtained from published studies and recent measurements of northern hemisphere static chamber (SC) measurements at 10 sites and eddy covariance (EC) measurements at 10 sites, of which 8 are in Alaska (Supplement Table S1). The eddy covariance measurements in Alaska (Fig. S2) are obtained at the Barrow Environmental Observatory (BEO1) tower operated by the Next Generation Ecosystem Experiment (NGEE)-Arctic group; Barrow Environmental Observatory tower (BEO2), Biocomplexity Experiment South (BES) tower, Climate Monitoring and Diagnostics Laboratory (CMDL) tower, Atqasuk (ATQ) tower and Ivotuk (IVO) tower operated by Global Change Research Group at San Diego State University (Zona et al., 2016); tower in Fairbanks (FAI, Iwata et al., 2015) operated by International Arctic Research Center, the University of Alaska Fairbanks; and tower at the Imnavait Creek watershed (IMN, Euskirchen et al., 2012). Monthly means are calculated across each observational record to compare to predicted mean seasonal $CH_4$ cycle. We discarded the monthly mean if the number of valid measurement days is less than half a month.

### 2.2.2 Comparisons to Airborne Measurements

The regionally integrated $CH_4$ mole fraction enhancements over Alaska were calculated from the $CH_4$ mole fractions measured by NOAA and Harvard Picarro spectrometers aboard a NASA C-23B aircraft (N430NA) during CARVE aircraft flights (Chang et al., 2014). The Harvard $CH_4$ measurements were gap filled with the NOAA $CH_4$ measurements to create a continuous 5-s time series. The flight measurements were conducted on selected days from May to September in 2012 and April to October in 2013 during the Carbon in Arctic Reservoirs Vulnerability Experiment (CARVE) campaign, for a total of 31 flight days in 2012 and 43 flight days in 2013 (Fig. S1 and Table S2). The measurements of $CH_4$ with concurrent CO mole fractions above 150 ppb are excluded to remove possible $CH_4$ production from biomass burning. In Alaska, atmospheric boundary layer depth is in the range of 1100-1600 m above ground level (agl) during April and October according to COSMIC satellite and Radiosonde data

(Chan and Wood, 2013). We assume that the observed concentration fluctuations below 500m agl can be used to infer the variation of surface $CH_4$ fluxes; the measurements above 1600 m agl are used to infer background mole fraction of $CH_4$. The monthly mean enhancements in observed atmospheric $CH_4$ mole fraction is compared to that estimated from the CLM4.5 $CH_4$ enhancements.

### 2.2.3 Comparisons to Global-Scale Inversions

To compare our methane emissions with global and regional scale inversions, we use monthly regional $CH_4$ emissions predicted by CarbonTracker (Peters et al., 2007; Bruhwiler et al., 2014) at 1°×1° resolution. In CarbonTracker estimates, the natural $CH_4$ emissions correspond to wetlands, soils, oceans, insects, and wild animals. To examine the land $CH_4$ emissions only, we apply the CLM land mask to exclude the inferred CarbonTracker $CH_4$ emission from the ocean surface. CarbonTracker $CH_4$ estimates are available from January 2000 through December 2010; we therefore limit comparisons against the CLM4.5 predictions to this period.

## 3 Results and Discussion

### 3.1 Model constraints and comparison with observations

We performed sensitivity analyses of all the parameters affecting seasonal $CH_4$ production, oxidation, and emission pathways and found that the parameterization of aerenchyma transport has the greatest impact on the seasonal $CH_4$ emissions in saturated areas. The $CH_4$ surface flux sensitivity to aerenchyma is most sensitive to aerenchyma area in saturated conditions, and decreases with increasing aerenchyma area, because increased $O_2$ fluxes through aerenchyma cause more $CH_4$ oxidation in the rhizosphere (Riley et al., 2011). Meng et al. (2012) tested plant functional type (pft)-specific fine root carbon ($C_{FR}$) as a proxy of aerenchyma area and found that aerenchyma area dependence on $C_{FR}$ leads to about 39% increases in global annual $CH_4$ emissions. In that study, an early spring spike in $CH_4$ emission through aerenchyma transport was shown at a Michigan site in both LAI and $C_{FR}$ based aerenchyma area. Our analysis shows that the simulated $CH_4$ burst through aerenchyma transport during spring thaw is very common in areas experiencing winter dormancy. In CLM4.5, $CH_4$ production in a given volume of soil is proportional to heterotrophic respiration (HR) in that soil volume, adjusted by soil temperature, pH, redox potential, and variation of seasonal inundation fraction. In the model, $CH_4$ production starts when the soil temperature is above the freezing point. However, CLM4.5 LAI lags behind the primary thaw day, which, because the original representation of aerenchyma in CLM4.5 is tied directly to LAI, results in a very low aerenchyma area and thus low aerenchyma transport of $O_2$ into the soil during spring thaw period. Only a very small portion of the $CH_4$ produced in the soil column is oxidized, allowing a large fraction of $CH_4$ to be transported to the surface by aerenchyma. The low oxidation rate also occurs when aerenchyma area is calculated with $C_{FR}$.

The uncertainty in representing the seasonality of aerenchyma area is due to (1) poor current understanding of root dynamics and their control on aerenchyma area and (2) scant relevant observations. In tundra, the aboveground production is often not a good

proxy for belowground production, because the soil temperature peaks later in the growing season than solar irradiance (Sullivan and Welker, 2005; Sloan, 2011). Further, root dynamics are strongly species dependent. Root growth of *Eriophorum angustifolium* may not be delayed when soil temperature is near 0°C (Chapin, 1974; Billing et al., 1977), while *Dupontia Fischeri* produces many fewer root tips at these low temperatures. In *Eriophorum vaginatum*, fine root growth is lagged significantly behind the aboveground spring growth flush (Kummerow and Russell, 1980).

To eliminate the possible bias in the seasonal variation of roots and the extremely low oxidation rate which caused CLM4.5 to predict a large $CH_4$ burst from inundated areas during the spring thaw, we modified the model parameter *S* to be constant, which is used in the aerenchyma area estimation. We constrained *S* using global total $CH_4$ emissions estimated by top-down and bottom-up simulations during 2000-2009 (Kirschke et al., 2013) and site-level measurements. We exclude the $CH_4$ emission from non-inundated areas for the analysis of seasonal dynamics because the model shows very small seasonal contribution of $CH_4$ emissions from non-inundated areas globally (Fig. 1). This $CH_4$ emission pulse from non-inundated areas, which may be related to soil moisture anomalies during spring thaw, has not been experimentally validated, but can lead to large biases in simulated $CH_4$ emissions from northern high latitudes (>50°N) in May and June (Fig. 1a and 1b). This simplification of the model produced seasonal cycles that did not contain the large springtime $CH_4$ emission bursts, and we therefore used this modified version for all experiments here.

We assessed the sensitivity of the modeled $CH_4$ fluxes to parametric uncertainty in the constant dimensionless factor *S*, as described above. *S* has a direct effect on the magnitude of modeled $CH_4$ emissions via its control of oxygen diffusion through the soil column and thus $CH_4$ oxidation. When $S = LAI$, the very low *LAI* in the spring thaw period leads to low oxidation and consequently overestimated $CH_4$ net emissions compared to CarbonTracker predictions. During the growing season, the model overestimates *LAI* at high latitude (Tian et al., 2004) leading to high oxidation and consequently underestimated net $CH_4$ emissions (Fig. 1e and f). However, few observations of aerenchymous tissue biomass are available to provide an *a priori* constraint to this value. Our goal here is to use a reasonable value of this parameter, not to fully characterize the uncertainty of the parameter choice on $CH_4$ emissions.

Based on a comparison of the globally integrated $CH_4$ flux with other global estimates, we choose $S$=4, which resulted in an estimated annual total $CH_4$ emission of 228 [Inter-annual Variability (IAV): 221- 239] Tg $CH_4$ $yr^{-1}$ with $F_{def}$ and 206 [IAV: 200-217] Tg $CH_4$ $yr^{-1}$ with $F_{S+G}$ during the period 2000 - 2009. The top-down and bottom-up models provide estimates of $CH_4$ emissions from natural wetlands of 175 [IAV: 142-208] Tg $CH_4$ $yr^{-1}$ and 217 [IAV: 177-284] Tg $CH_4$ $yr^{-1}$, respectively, during the same period (Kirschke et al., 2013). The mean $CH_4$ emission predicted by CLM4.5 is about 42 Tg $CH_4$ $yr^{-1}$ lower than the original CLM4Me prediction (annual mean of 270 Tg $CH_4$ $yr^{-1}$ from 1948 to 1972), but slightly larger than the mean value from other bottom-up and top-down models. The disagreement between studies with different models is as large as 66% (Kirschke et al., 2013), hence our estimate is well within the range of values from top-down constraints and underscores the uncertainty involved in using such a constraint in inferring model parameters.

Compared with CarbonTracker predictions, CLM's biases of underestimated growing-season $CH_4$ emissions north of 56°N and biases of overestimated $CH_4$ emissions in 2-53°N and 34-56°S are reduced when using $S = 4$ compared to the default parameterization (Fig. 1d and f). For the global zonal mean, the CLM $CH_4$ prediction biases are reduced with $F_{S+G}$ (RMSE=2.5 mg $CH_4$ $m^{-2}$ $day^{-1}$) compared with $F_{def}$ (RMSE = 3.1 mg $CH_4$ $m^{-2}$ $day^{-1}$). With $F_{S+G}$, the biases are much reduced in 2-50°N and 30-58°S. However, negative $CH_4$ emission biases in the tropics remain (Fig. 1c and 1e). The differences in $CH_4$ emissions using SWAMPS-GLWD and CLM4.5 predicted inundation fraction implies that the prediction uncertainties are not only from the biogeochemical parameterization but also from the wetland extent, consistent with several recent model inter-comparison analyses (Melton et al., 2013; Bohn et al., 2015). In Alaska, the predicted annual $CH_4$ emissions between 2000 and 2010 are 1.47±0.20, 1.58±0.07, and 1.12±0.05 Tg $CH_4$ $yr^{-1}$ for CarbonTracker, CLM4.5 with $F_{S+G}$, and CLM4.5 with $F_{def}$, respectively. Although our predicted annual emissions are reasonable compared with most land surface model predictions, the May to September predictions are about 50-70% of the emissions estimated using an atmospheric inversion based on CARVE observations of 2.1± 0.5 Tg $CH_4$ $yr^{-1}$ (Chang et al., 2014).

## 3.2 Seasonal $CH_4$ emissions

### 3.2.1 Site level comparison

The mean seasonal cycle of predicted $CH_4$ emissions is calculated from the 2000-2012 monthly mean in a 0.5°×0.5° grid cell where site measurements exist, while the seasonal cycle of site measurements is calculated for the measurement years. If multiple measurement sites and multiple measurement years with the same measurement method (SC or EC) exist within a given grid cell, the observations are averaged to create a grid cell mean value that can be directly compared with the modeled value for that grid cell. In the 10 site-level static chamber measurements at saturated sites (Fig. 2a-l), the seasonality is well predicted by the revised CLM4.5 $CH_4$ model at most sites. Measurements and predictions show the peak emission month to be July or August at most sites, except the site in Michigan, USA (Fig. 2f) where the model successfully predicted the peak emissions in May. However, the model misrepresents the seasonality at the Stordalen (Sweden) (Fig. 2a and k) and the Boreas NSA (Canada) (Fig. 2i) site. At the Ruoergai (China) (Fig. 2j), the model does not show a strong seasonal variation from April to September, and notably underestimates the growing season $CH_4$ emissions. The underestimation of growing season emissions is also found in the Minnesota (USA), Michigan (USA), and Boreas NSA (Canada) sites (Fig. 2d, 2e, 2f and 2h). The sites experiencing soil frost with valid measurements in the cold season demonstrate the CLM4.5 underestimation of $CH_4$ emissions during this period (Fig. 2a, 2d, 2e and 2i).

The eddy covariance measurements from four sites, the BEO1, BEO2, BES, and CMDL sites are in the same model grid cell, therefore, the measurements in these four sites are aggregated to the same grid cell as that of Alaska (Fig. 2m). As the footprints of the measurement towers were not estimated, all the modeled $CH_4$ emissions at eddy covariance sites are weighted with an observationally estimated seasonal-invariant range of inundation faction: Stordalen: 80-100%; Boreas SSA: 50-90%; Barrow: 60-100%;

Atqasuk: 10-30%; Ivotuk: 5-25%; Fairbanks: 0.5-2.5% and IMN: 5-25%. Measurements at the Stordalen site (Fig. 2a and k) show very different $CH_4$ emission patterns in seasonality and magnitude for different years and measurement methods. The model significantly underestimates $CH_4$ emissions even with the maximum fraction of inundation in Stordalen (Fig. 2k). In comparison with the static chamber measurements at Alaska (Fig. 2h), the model predicts a much shorter $CH_4$ emission season at the non-inundated sites (Fig. 2m-q). The estimated $CH_4$ emissions begin in April at Ivotuk, Fairbank, and Imnavait. At the northern sites, Barrow and Atqasuk, the estimated $CH_4$ emissions begin in May. In the short emission season, the model underestimates $CH_4$ emissions in June and July at Barrow and Atqasuk and in July at Imnavait, even with the maximum inundation estimation. While the cold-season measurements at Barrow, Atqasuk, and Ivotuk show large $CH_4$ emissions from October to April in agreement with the static chamber measurements at the sites with cold season soil frost, predicted $CH_4$ emissions end in October at all the Alaskan sites. The largest monthly mean emissions in Alaska cold season are 24.8±9.0 mg $CH_4$ $m^{-2}$ $day^{-1}$ measured in October at Ivotuk.

A number of factors affect the correspondence between site-level $CH_4$ emission observations and CLM4.5 predictions (Fig. 2), including: (1) we used reanalysis climate forcing data which may lead to some of the differences with the site observations; (2) we used the model's default surface characterization, which is unlikely to exactly match the actual vegetation and soil properties; (3) the spatial and temporal coverage of the site data are sparse; (4) the inter-annual variation of wetland $CH_4$ emission can be significant; (5) the method of measuring $CH_4$ fluxes varied from site to site and (6) the seasonal fraction of inundation in eddy covariance tower footprint is unknown. We also expect differences between our CLM4.5 predictions and those reported in Riley et al., (2011) at the site-level comparison, because: (1) simulations in this study were done at higher resolution (0.5°x0.5°) than those in Riley et al. (2011) (1.9° x2.5°); (2) the current simulations are forced by CRUNCEP climate, while Riley et al., (2011) simulations were forced with Qian et al., (2006) climate; (3) the *S* parameter is changed, as discussed above; and (4) the overall water and carbon cycles of CLM changed substantially between CLM4.0 and CLM4.5 (Koven et al., 2013). The site-level discrepancies occur because of the uncertainties discussed above and those arising from other parameters (Riley et al., 2011), including: $Q_{10}$ of $CH_4$ production and oxidation, $CH_4$ half-saturation oxidation coefficient, $O_2$ half-saturation oxidation coefficient, maximum oxidation rate of $CH_4$ oxidation, and impact of pH and redox potential on $CH_4$ production.

### 3.2.2 Regional $CH_4$ emissions comparison

The biases between CLM4.5 and CarbonTracker $CH_4$ emissions vary with latitude (Fig. 3). The aggregated $F_{S+G}$ led to larger $CH_4$ emission biases in Alaska (RMSE = 4 mg $CH_4$ $m^{-2}$ $day^{-1}$) compared to the $CH_4$ prediction with $F_{def}$ (RMSE = 3 mg $CH_4$ $m^{-2}$ $day^{-1}$), although it led to smaller global $CH_4$ emission biases. In Alaska between 58-66°N during the growing season, CLM4.5 using $F_{def}$ has good agreement with CarbonTacker predictions. In this region, $CH_4$ emissions begin in May, peak in July and August, and end in October (Fig. 4). In May and June, CarbonTacker shows a weak $CH_4$ sink (~O[$10^{-2}$-$10^{-1}$] mg $CH_4$ $m^{-2}$ $day^{1}$) in contrast to a CLM4.5 predicted weak $CH_4$ source (~O[$10^{-1}$] mg $CH_4$ $m^{-2}$ $day^{-1}$) with $F_{def}$ and stronger $CH_4$ source (~O[1] mg $CH_4$ $m^{-2}$ $day^{-1}$) with

$F_{S+G}$ in the interior region of Alaska (Interior Alaska) between 63°N-66°N . We hypothesize that this discrepancy occurs because of the difference in the two wetland datasets and the accounting of $CH_4$ emissions from the non-inundated areas in CarbonTracker. Net $CH_4$ consumption occurs at dry sites where oxygen is available in the top soil layers (Wickland et al., 1999); however, $CH_4$ fluxes from the non-inundated areas which could be substantial (Zona et al., 2016) are excluded in CLM4.5 predictions shown in Fig. 3, as described in Methods. Interior Alaska has a highly continental climate with warm and relatively dry summers and extremely cold winters. The weak $CH_4$ source in the dry summer is thus caused by a reduced wetland extent in Interior Alaska. Interior Alaska experiences the most rain events in autumn, mainly in August and September (Hinzman et al., 2006), which restores some of the extent of wetlands and leads to increases in $CH_4$ emissions in August and early September. CarbonTracker successfully represented the restored wetland in August and September but not CLM4.5 (Fig. 3 and 4). The autumn emission period is very short and ends with the onset of winter, resulting in a strong drop in $CH_4$ emissions in October.

The CLM4.5 underestimation of northern (> 68°N) Alaska site-level $CH_4$ emissions during the growing season at some sites is confirmed with comparison to CarbonTracker inversions (Fig. 3b). In southern and northern coastal Alaska, CLM4.5 predicts a much shorter $CH_4$ emission season and a smaller magnitude of $CH_4$ emissions than CarbonTracker. The period of the largest underestimation by CLM4.5 is from May to July with the maximum underestimation of about 9.2 mg $CH_4$ $m^{-2}$ $day^{-1}$ in June. The underestimated $CH_4$ emissions occur with both $F_{S+G}$ and $F_{def}$ in the north of 68°N. During the cold season from October to April, CLM4.5 predictions with $F_{S+G}$ or $F_{def}$ are consistently smaller than CarbonTracker estimates across all the latitudes. The mean underestimation of cold season $CH_4$ emission is less than 1 mg $CH_4$ $m^{-2}$ $day^{-1}$, which is much smaller than the underestimation we found compared to site level measurements. In comparison with CarbonTracker, CLM4.5 predicted 0.46±0.07Tg and 0.39±0.08Tg less Alaska wide $CH_4$ emissions in cold season (October to April) with $F_{S+G}$ and $F_{def}$, respectively.

The CarbonTracker inversions suggest 21.9±3.2% of the annual Alaska $CH_4$ emissions occur during the cold season, while CLM4.5 predicts only 3.5±1.3% and 8.3±3.0% (with $F_{def}$ and $F_{S+G}$, respectively) occur during the cold season. When September and April are included in the "cold season", the contribution is increased to 45.3±4.5% by CarbonTracker, which is slightly smaller than the cold season contribution (50±9%) inferred from site-level (BEO2, BES, CMDL, ATQ and IVO) measurements (Zona et al., 2016). The September-April contributions to annual emissions predicted by CLM4.5 are 32.1±8.1% and 40.1±14.7% of the predicted annual emissions with $F_{S+G}$ and $F_{def}$, respectively. Although $CH_4$ fluxes from the ocean surface are excluded, we cannot exclude some influence of coastal grid cells on the CarbonTracker estimates.

The atmospheric $CH_4$ mole fraction enhancements calculated from CLM4.5 predicted $CH_4$ emissions are lower than the CARVE measured $CH_4$ mole fraction enhancements (Fig. 5). However, in contrast to the emission underestimations that only occur from May to July, the monthly atmospheric $CH_4$ mole fraction enhancements are underestimated throughout the year, with a maximum underestimation in August (Fig. 5a). The CARVE measured peak mole fraction enhancement due to surface $CH_4$

emissions is in August for both 2012 and 2013. Although CLM4.5 predicted the peak $CH_4$ mole fraction enhancement in August, 2012, predicted seasonal $CH_4$ mole fraction enhancements are much smaller in 2013 and peaks in September. The underestimation of cold season mole fraction $CH_4$ enhancements by CLM4.5 leads to 24.0±9.2 ppb and 18.9±17.3 ppb lower $CH_4$ mole fraction enhancements in April and October 2013, respectively. From April to October, the two-year mean monthly atmospheric $CH_4$ mole fraction enhancements are underestimated by 15 ppb in WRF-STILT-CLM model predictions. The underestimation may not be attributed to anthropogenic $CH_4$ source and agricultural waste because: (1) we excluded both observed and modeled $CH_4$ mole fraction enhancements when [CO]>150 ppb, given that anthropogenic $CH_4$ mole fraction enhancements are consistently correlated to CO mole fraction enhancements (Zona et al., 2016) and (2) The $CH_4$ emissions from agricultural waste does not show strong seasonal variation according to CarbonTracker estimates. The large standard deviation of CARVE observed $CH_4$ mole fraction enhancements implies that the $CH_4$ emissions have large spatial and temporal variability. The CLM4.5 predictions are generally within the observed range of variation except in April and May in 2013.

The very low cold season $CH_4$ emission predictions at site and regional scales occurs because of the assumed temperature sensitivity for $CH_4$ production when the soil temperature of a given layer is at or below freezing (i.e., no $CH_4$ production occurs in that soil layer). The multi-layer structure of CLM4.5 can in principle generate $CH_4$ emissions deeper in the soil after the surface has frozen, though even then, modeled diffusion rates through frozen surface layers are low. Although the measurements show winter $CH_4$ emissions, it remains uncertain whether these emissions are from production at low temperature or residual $CH_4$ from the end of the growing season. Understanding which of these is occuring is important for diagnosing how to improve model representation of the processes responsible for the wintertime fluxes. The cold season underestimation by CLM4.5 is also partly attributed to the low wetland area during this period at high latitudes (currently, $F_{def}$ is set to zero when snow is present). Given the current observations of $CH_4$ emissions during the cold season, we believe these two factors need to be re-evaluated in CLM4.5.

### 3.3 Interannual variation of $CH_4$ cycle

The CLM4.5 simulated Alaska $CH_4$ emissions using $F_{def}$ are in very good agreement with CarbonTracker-$CH_4$ emission in the growing season but biased in the cold season (Fig. 6). The largest growing season discrepancies occur in 2006 and 2007. Bruhwiler et al. (2014) attributed the CarbonTracker 2007 $CH_4$ emission anomaly to warmer temperatures and higher than normal precipitation. However, the CRUNCEP reanalysis data we used to force CLM4.5 do not have a positive precipitation anomaly in either 2006 or 2007 (Fig. 7a). In contrast, there is a strong negative precipitation anomaly in 2007. The obvious wet years (2000, 2005, 2008, 2011 and 2012) in the CRUNCEP reanalysis data are not directly related to the predicted and measured wetland area anomaly or $CH_4$ emission anomaly. The mean air temperature in 2007 is only slightly higher than 2000-2012 mean air temperature (Fig. 7b). The correlation analysis implies that the model predicted interannual $CH_4$ variation is mainly explained by temperature variation (Fig. 8a, r=0.86, P=0.0007), followed by the default wetland extent ($F_{def}$) variation (Fig. 8b, r=0.65, P=0.03), but weakly explained by SWAMPS-GLWD

wetland extent ($F_{S+G}$) variation (r=0.44, P=0.17) and precipitation variation (r=0.18, P=0.58). When the $CH_4$ predictions are calculated with $F_{S+G}$, correlation between the interannual variation of $CH_4$ and variation in $F_{S+G}$ (r=0.18, P=0.59), precipitation (r=0.36, P=0.29), and temperature (r=0.32, P=0.33) are substantially reduced. Interannual variation of $CH_4$ emissions by CarbonTracker are not well correlated to SWAMPS-GLWD wetland extent variation (r=0.33, P=0.32), variations in CRUNCEP temperature (r=-0.23, P=0.49), or precipitation (r=-0.06, P=0.86).

## 4 Concluding remarks

We implemented and tested needed changes to the estimate of aerenchyma area in CLM4.5. The modeled and measured $CH_4$ emissions and enhancements in atmospheric mole fractions of $CH_4$ are used to analyze the seasonal wetland $CH_4$ emission cycle in Alaska. Both the measurements and model predictions show large latitudinal variability of $CH_4$ seasonal cycles. At the site level, CLM4.5 generally captures the seasonality in growing season $CH_4$ emissions. However, comparing eddy covariance $CH_4$ observations with the model predictions is complicated by the unknown fraction of inundation in the footprint of the measurement tower, which may cause large variations in $CH_4$ emission predictions. Measurements from the sites experiencing wintertime soil frost imply that $CH_4$ emissions continue in the cold season (October to April). The likely incorrect treatment of $CH_4$ production under soil frost in CLM4.5 leads to underestimates of the wintertime emissions. This conclusion is confirmed by the discrepancies between CLM4.5 and CarbonTracker predictions, although the cold season discrepancies between CLM4.5 and CarbonTracker are much smaller than the discrepancies between CLM4.5 and site-level measurements. The differences between the seasonality predicted by CLM4.5 and CarbonTracker vary with time and latitude, although the Alaska area-integrated $CH_4$ emissions agree well. Besides the strength of wintertime $CH_4$ emissions, the main discrepancies between CLM4.5 and CarbonTracker estimates are northern and southern coastal area $CH_4$ emissions. The inundation area leads to uncertainties in predictions of seasonal and interannual variability of $CH_4$ emissions. Compared with the CLM4.5 predicted inundation area, the aggregated $F_{S+G}$ inundation led to smaller global $CH_4$ emission biases than $F_{def}$ (RMSE dropped from 3.1 mg $CH_4$ $m^{-2}$ $day^{-1}$ to 2.5 mg $CH_4$ $m^{-2}$ $day^{-1}$) between CLM4.5 and CarbonTracker. In contrast, the $F_{S+G}$ inundation area increased seasonal emission biases in Alaska by increasing RMSE from 3 to 4 mg $CH_4$ $m^{-2}$ $day^{-1}$ compared with the CLM4.5 predicted inundation. The larger SWAMPS-GLWD inundation area leads to much stronger Alaska wide annual $CH_4$ emissions compared to those calculated from the default predicted inundation area. CLM4.5 predictions show that the interannual variations of $CH_4$ emissions are correlated with the reanalysis air temperature and wetland extent variation. In contrast, interannual variation in CarbonTracker $CH_4$ emissions is weakly related to interannual variation in SWAMPS-GLWD wetland area and reanalysis precipitation and temperature.

The CLM4.5 $CH_4$ module constrained from global total annual $CH_4$ emissions does not accurately represent the seasonal cycles at the regional and site scale seasonal cycles due to large temporal and spatial heterogeneity in surface $CH_4$ emissions and wetland extent. Further improving the $CH_4$ biogeochemical model at the seasonal and annual time scales requires further extensive experiments to better understand climate controls on above- and below-ground physiological processes and how vegetation

controls gaseous transport (e.g. $CH_4$ production under low temperatures). Although cold season site-level measurements are rare, the large discrepancies in winter emissions between CLM4.5 and CarbonTracker predictions and site measurements indicate that studies on winter ecosystem activities and wetland evolution in high latitude would be valuable.

**Acknowledgements**: Funding for this study was provided by the US Department of Energy, BER, under the RGCM program and NGEE-Arctic project under contract # DE-AC02-05CH11231. We thank the CARVE flight group for efforts on CARVE science flights. CarbonTracker $CH_4$ results provided by NOAA ESRL, Boulder, Colorado, USA from the website at http://www.esrl.noaa.gov. The eddy covariance tower data used in this study were supported by the Division of Polar Programs of the National Science Foundation (NSF) (Award 1204263); Carbon in Arctic Reservoirs Vulnerability Experiment (CARVE), an Earth Ventures (EV-1) investigation, under contract with the National Aeronautics and Space Administration; and Department of Energy (DOE) Grant DE-SC005160. Logistical support was funded by the NSF Division of Polar Programs.

## References


Alavala, P. C. and Kirchoff, V. W. J. H.: Methane fluxes from the Pantanal floodplain in Brazil: Seasonal variation, in: Non-$CO_2$ Greenhouse Gases: Scientific understanding, control and implementation, edited by: Goossens, A., De Visscher, A., Boeckx, P., and Van Cleemput, O., Kluwer Academic Publishers, Netherlands, 95–99, 2000.

Bartlett, K. B., Crill, P. M., Sass, R. L., Harriss, R. C., Dise, N. B.: Methane emissions from tundra environments in the Yukon-Kuskokwim delta, Alaska, J. Geophys. Res., 97D, 16645–16660, 1992.

Bergamaschi, P., Frankenberg, C., Meirink, J. F., Krol, M., Villani, M. G., Houweling, S., Dentener, F., Dlugokencky, E. J., Miller, J. B., Gatti, L. V., Engel, A., and Levin, I.: Inverse modeling of global and regional $CH_4$ emissions using SCIAMACHY satellite retrievals, J. Geophys. Res.-Atmos., 114, D22301, doi:10.1029/2009JD012287, 2009.

Billings, W. D., Peterson, K. M., Shaver, G. R., Trent, A. W.: Root growth, respiration, and carbon dioxide evolution in an Arctic tundra soil. Arctic Alpine Res., 9, 129–137, 1977.

Bohn, T. J., Melton, J. R., Ito, A., Kleinen, T., Spahni, R., Stocker, B. D., Zhang, B., Zhu, X., Schroeder, R., Glagolev, M. V., Maksyutov, S., Chen, G., Denisov, S. N., Eliseev, A. V., Gallego-Sala, A., McDonald, K. C., Rawlins, M. A., Subin, Z. M., Tian, H., Zhuang, Q., Kaplan, J. O.: WETCHIMP-WSL:intercomparison of wetland methane emissions models over West Siveria, Biogeosciences, 12, 3321-3349, 2015.

Brouchkov, A., Fukuda, M., Tomita, F., Asano, K., Tanaka, M.: Microbiology and gas emission at low temperatures: some field and experimental results. Töhoku Geophys. Journ., 36, 452-455, 2003.

Bruhwiler, L., Dlugokencky, E., Masarie, K., Ishizawa, M., Andrews, A., Miller, J., Sweeney, C., Tans, P., Worthy, D.: CarbonTracker-$CH_4$: an assimilation system for estimating emissions of atmospheric methane, Atmos. Chem. Phys., 14, 8269-8293, 2014.

Bubier, J. L., Crill, P. M., Varner, R. K., and Moore, T. R.: BOREAS TGB-01/TGB-03 $CH_4$ chamber flux data: NSA Fen. Data set, available at: http://www.daac.ornl.gov, Oak Ridge, TN, USA, 1998.

Chan, K. M., Wood, R.: The seasonal cycle of planetary boundary layer depth determined using COSMIC radio occultation data, J. Geophys. Res.-Atmos., 118, 12,422-12,434, doi:10.1002/2013JD020147, 2013.

Chang, R. Y. W, Miller, C. E., Dinardo, S. J., Karion, A., Sweeney, C., Daube, B., Henderson, J. M., Mountain, M. E., Eluszkiewicz, J., Miller, J. B., Bruhwiler, L. M. P., Wofsy, S. C.: Methane emissions from Alaska in 2012 from CARVE airborne observations. Proc. Natl. Acad. Sci., 111, 16694-16699, 2014.

Chapin, F. S.: Morphological and physiological mechanisms of temperature compensation in phosphate absorption along a latitudinal gradient, Ecology, 55, 1180-1198, 1974.

Clein, J. S., Schimel, J. P.: Microbial activity of tundra and taiga soils at sub-zero temperatures. Soil. Biol. Biochem., 29(9), 1231-1234, 1995.

Clement, R. J., Verma, S. B., and Verry, E. S.: Relating Chamber Measurements to Eddy-Correlation Measurements of Methane Flux, J. Geophys. Res.-Atmos., 100, 21047–21056, 1995.

Comas, X., Slater, L., Reeve, A.: Seasonal geophysical monitoring of biogenic gases in a northern peatland: implications for temporal and spatial variability in free phase gas

production rates, J. Geophys. Res. Biogeosci. 113, G01012, doi:10.1029/2007JG000575, 2008.
Ding, W. X., Cai, Z. C., and Wang, D. X.: Preliminary budget of methane emissions from natural wetlands in China, Atmos. Environ., 38, 751–759, doi:10.1016/J.Atmosenv.2003.10.016, 2004.
Dise, N. B.: Methane Emission from Minnesota Peatlands-Spatial and Seasonal Variability, Global Biogeochem. Cy., 7, 123–142, 1993.
Dunfield P, Knowles R, Dumont R, Moore TR. Methane production and consumption in temperate and subarctic peat soils: Response to temperature and pH. Soil Biol Biochem 1993; 25: 321–326.
Euskirchen, E. S., Bret-Harte, M. S., Scott, G. J., Edgar, C., Shaver, G. R.: Seasonal patterns of carbon dioxide and water fluxes in three representative tundra ecosystems in northern Alaska, Ecosphere, 1-19, 2012.
Granberg, G., Ottosson-Lofvenius, M., Grip, H., Sundh, I., and Nilsson, M.: Effect of climatic variability from 1980 to 1997 on simulated methane emission from a boreal mixed mire in northern Sweden, Global Biogeochem. Cycles, 15, 977–991, 2001.
Harazono, Y., Mano, M., Miyata, A., Yoshimoto, M., Zulueta, R. C., Vourlitis, G.L., Kwon, H., Oechel, W.: Temporal and spatial differences of methane flux at arctic tundra in Alaska, Natl Inst. Polar Res, Spec. Issue, 59:79–95, 2006.
Hargreaves, K. J., Fowler, D., Pitcairn, C. E. R. and Aurela, M.: Annual methane emission from Finnish mires estimated from eddy covariance campaign measurements, Theor. Appl. Climatol. 70, 203–213, 2001.
Henderson, J. M., Eluszkiewicz, J., Mountain, M. E., Nehrkorn, T., Chang, R. Y.-W., Karion, A., Miller, J. B., Sweeney, C., Steiner, N., Wofsy, S. C., Miller, C. E., Atmospheric transport simulations in support of the Carve in Arctic Reservoirs Vulnerability Experiment (CARVE), Atmos. Chem. Phys., 15,4093-4116, 2015.
Hinzman, L.D., L. A. Viereck, P. Adams, V. E. Romanovsky, and K. Yoshikawa, 2006. Climate and permafrost dynamics of the Alaskan boreal forest. In Alaska's changing boreal forest. Edited by F.S. Chapin III, M.W. Oswood, K Van Cleve, L.A. Viereck, and D.L. Verbyla. Oxford University Press, New York. pp. 39-61.
Hommeltenberg, J., Mauder, M., Drösler, M., Heidbach, K., Werle, P., Schmid, H. P.: Ecosystem scale methane fluxes in a natural temperature bog-pine forest in southern Germiny, Biogeosciences, 11, 3477-3493, 2014.
Hugelius, G., Strauss, J., Zubrzycki, S., Harden, J. W., Schuur, E. A. G., Ping, C.-L., Schirrmeister, L., Grosse, G., Michaelson, G. J., Koven, C. D., O'Donnell, J. A., Elberling, B., Mishra, U., Camill, P., Yu, Z., Palmtag, J., Kuhry, P.: Estimated stocks of circumpolar permafrost carbon with quantified uncertainty ranges and identified data gaps, Biogeosciences, 11, 6573-6593, 2014.
IPCC: Climate Change 2007: The Physical Science Basis. Contribution of Working Group I to the Fourth Assessment Report of the IPCC, edited by: Solomon, S., Qin, D., Manning, M., Chen, Z., Marquis, M., Averyt, K. B., Tignor, M., and Miller, H. L., Cambridge University Press, Cambridge, United Kingdom and New York, 2007.
Iversen, C. M., Sloan, V. L., Sullivan, P. F., Euskirchen, E. S., McGuire, A. D., Norby, R. J., Walker, A. P., Warren, J. M., Wullschleger, S. D.:The unseen iceberg: plant roots in arctic tundra, New Phytologist, 205, 34-59, doi: 10.1111/nph.13003, 2015.
Iwata, H., Harazono, Y., Ueyama, M., Sakabe, A., Nagano, H., Kosugi, Y., Takahashi, K.,

Kim, Y.: Methane exchange in a poorly-drained black spruce forest over permafrost observed using the eddy covariance technique, Agric. For. Meteorol., 214-215, 157-168 2015.
Jackowicz-Korczyński, M., Christensen, T. R., Bäckstrand, K., Crill, P., Friborg, T., Mastepanov, M., Ström, L.: Annual cycle of methane emission from a subarctic peatland, J. Geophys. Res., 115, G02009, doi:10.1029/2008JG000913, 2010.
Juutinen, S., Alm, J., Larmola, T., Huttunen, J. T., Morero, M., Martikainen, P. J., Silvola, J.: Major implication of the littoral zone for methane release from boreal lakes, Global Biogeochem. Cycles, 17, 1117.10.1029/2003GB002105, 2003.
Karl, D. M., Tilbrook, B. D.: Production and transport of methane in oceanic particulate organic matter, Nature, 368, 732-734, 1994.
Keller, M. M.: Biological sources and sinks of methane in tropical habitats and tropical atmospheric chemistry, Princeton University, 1990.
King, J. Y., William, S. R., Shannon K. R.: Methane emission and transport by arctic sedges in Alaska: results of a vegetation removal experiment, J. Geophys. Res., 103, 29083-29092.
Kirschke, S., Bousquet, P., Ciais, P., Saunois, M., Canadell, J. G., Dlugokencky, E. J., Bergamaschi, P., Bergmann, D., Blake, D. R., Bruhwiler, L., Cameron Smith, P., Castaldi, S., Chevallier, F., Feng, L., Fraser, A., Heimann, M., Hodson, E. L., Houweling, S., Josse, B., Fraser, P. J., Krummel, P. B., Lamarque, J., Langenfelds, R. L., Le Quéré, C., Naik, V., O'Doherty, S., Palmer, P. I., Pison, I., Plummer, D., Poulter, B., Prinn, R. G., Rigby, M., Ringeval, B., Santini, M., Schmidt, M., Shindell, D. T., Simpson, I. J., Spahni, R., Steele, L. P., Strode, S. A., Sudo, K., Szopa, S., van der Werf, G. R., Voulgarakis, A., van Weele, M., Weiss, R. F., Williams, J. E., and Zeng, G.: Three decades of global methane sources and sinks, Nat. Geosci., 6, 813–823, doi: 10.1038/ngeo1955, 2013.
Koh, H. S., Ochs, C. A., and Yu, K. W.: Hydrologic gradient and vegetation controls on $CH_4$ and $CO_2$ fluxes in a spring-fed forested wetland, Hydrobiologia, 630, 271–286, doi:10.1007/S10750-009-9821-X, 2009.
Koven, C. D., Riley, W. J., Subin, Z. M., Tang, J. Y., Torn, M. S., Collins, W. D., Bonan, G. B., Lawrence, D. M., Swenson, S. C.: The effects of vertically resolved soil biogeochemistry and alternate soil C and N models on C dynamics of CLM4, Biogeosciences, 10, 7109-7131, 2013.
Kummerow, J., Russell, M.: Seasonal root growth in the Arctic tussock tundra, Oecologia, 47: 196–199, 1980.
Lupascu, M., Wadham, J. L., Hornibrook, E. R. C., Pancost, R. D.: Temperature sensitivity of methane production in the permafrost active layer at Stordalen, Sweden: A comparison with non-permafrost northern wetlands, Arct., Antarc., Alp. Res., 44(4), 469-482, 2012.
Mastepanov, M., Sigsgaard, C., Tagesson, T., Ström, L., Tamstorf, M. P., Lund, M., Christensen, T. R.: Revisiting factors controlling methane emissions from high-arctic tundra, Biogeosciences, 10, 5139-5158, 2013.
Mastepanov, M., Sigsgaard, C., Dlugokencky, E. J., Houweling, S., Ström L., Tamstorf, M. P., and Christensen, T. R.: Large tundra methane burst during onset of freezing, Nature, 456, 628–631, 2008.

747 Mao, J., Shi, X., Thornton, P. E., Hoffman, F. M., Zhu, Z., Myneni, R. B., Global
748 latitudinal-asymmetric vegetation growth trends and their driving mechanisms:2982-
749 2009, Remote Sens., 5 1484-1497, 2013.
750 McEwing, K. R., Fisher, J. P., Zona, D.: Environmental and vegetation controls on the
751 spatial variability of $CH_4$ emission from wet-sedge and tussock tundra ecosystem in
752 the Arctic, Plant Soil, 388, 37-52, 2015.
753 Melton, J. R., Wania, R., Hodson, E. L., Poulter, B., Ringeval, B., Spahni, R., Bohn, T.,
754 Avis, C. A., Beerling, D. J., Eliseev, A.V., Denisov, S. N., Hopcroft, P. O.,
755 Lettenmaier, D. P., Riley, W. J., Singarayer, J. S., Subin, Z. M., Tian, H., Zürcher,
756 Brovkin, V., van Bodegom, P. M., Kleinen, T., Yu, Z. C., Kaplan, J. O., Present state
757 of global wetland extent and wetland methane modeling: conclusions from a model
758 inter-comparison project (WETCHIMP), Biogeosciences, 10, 753–788,2013.
759 Meng, L., Hess, P. G. M., Mahowald, N. M., Yavitt, J. B., Riley, W. J., Subin, Z. M.,
760 Lawrence, D. M., Swenson, S. C., Jauhiainen, J., and Fuka, D. R.: Sensitivity of
761 wetland methane emissions to model assumptions: application and model testing
762 against site observations, Biogeosciences, 9, 2793–2819, doi:10.5194/bg-9-2793-
763 2012, 2012.
764 Mialon, A., Royer, A., Fily, M.: Wetland seasonal dynamics and interannual variability
765 over northern high latitudes, derived from microwave satellite data, J. Geophys. Res.,
766 110, D17102, doi:10.1029/2004JD005697, 2005.
767 Moosavi, S. C., Crill, P. M., Pullman, E. R., Funk, D. W., Peterson, K. M.: Controls on
768 $CH_4$ flux from an Alaskan boreal wetland, Global Biogeochem. Cycles, 10, 287-296,
769 1996.
770 Morin, T. H., Bohrer, G., Naor-Azrieli, L., Mesi, S., Kenny, W. T., Mitsch, W. J.,
771 Schäfer, K. V. R.: The seasonal and diurnal dynamics of methane flux at a created
772 urban wetland. Ecol. Engin., 72, 74-83, 2014.
773 Nakano, T., Kuniyoshi, S., Fukuda, M.: Temporal variation in methane emission from
774 tundra wetlands in a permafrost area, northeastern Siberia. Atmos. Environ., 34, 1205–
775 1213, 2000.
776 Olivas, P. C., Oberbauer, S. F., Tweedie, C., Oechel, W. C., Lin, D., Kuchy, A.: Effects
777 of Fine-Scale Topography on $CO_2$ Flux Components of Alaskan Coastal Plain Tundra:
778 Response to Contracting Growing Seasons, Arct. Antarct. Alpine Res., 43, 256–266,
779 doi: 10.1657/1938-4246-43.2.256, 2011.
780 Peters, W., Jacobson, A. R., Sweeney, C., Andrews, A. E., Conway, T. J., Masarie, K.,
781 Miller, J. B., Bruhwiler, L. M. P., Petron, G., Hirsch, A., Worthy, D. E. J., van der
782 Werf G. R., Randerson, J. T., Wennberg, P. O., Krol, M. C., Tans, P. P.: An
783 Atmospheric perspective on north American carbon dioxide exchange:
784 CarbonTracker, PNAS, 18925-18930, 2007.
785 Pickett-Heaps, C. A., Jacob, D. J., Wecht, K. J., Kort, E. A., Wofsy, S. C., Diskin, G. S.,
786 Worthy, D. E. J., Kaplan, J. O., Drevet, J.: Magnitude and seasonality of wetland
787 methane emissions from the Hudson Bay Lowlands (Canada), Atmos. Chem. Phys.,
788 11, 3773-3779, 2011.
789 Prigent, C., F. Papa, F. Aires, W. B. Rossow, E. Matthews.: Global inundation dynamics
790 inferred from multiple satellite observations, 1993-2000, J. Geophys. Res.-Atmos.,
791 112, D12107, doi:10.1029/2006JD007847, 2007.
792 Qian, T. T., Dai, A., Trenberth, K. E., and Oleson, K. W.: Simulation of global land

surface conditions from 1948 to 2004. Part I: Forcing data and evaluations, J. Hydrometeorol., 7, 953–975, 2006.
Riley, W. J., Subin, Z. M., Lawrence, D. M., Swenson, S. C., Torn, M. S., Meng, L., Mahowald, N. M., Hess, P.: Barriers to predicting changes in global terrestrial methane fluxes: analyses using CLM4Me, a methane biogeochemistry model integrated in CESM, Biogeosciences, 8, 1025-1953, 2011.
Ringeval, B., de Noblet-Ducoudré, N., Ciais, P., Bousquet, P., Prigent, C., Papa, F., Rossow, W. B.: An attempt to quantify the impact of changes in wetland extent on methane emissions on the seasonal and interannual time scales, Global Biogeochem. Cycles, 24, GB2003, doi:10.1029/2008GB003354, 2010.
Rinne, J., Riutta, T., Pihlatie, M., Aurela, M., Haapanala, S., Tuovinen, J., Tuittila, E.: Annual cycle of methane emission from a boreal fen measured by the eddy Covance technique., Tellus, 59B, 449-457, 2007.
Roulet, N. T., Ash, R., Moore, T.R.: Low boreal wetlands as a source of atmospheric methane, J. Geophys. Res., 97 (D4), 3739-3749, 1992.
Saarnio, S., Alm, J., Silvola, J., Lohila, A., Nykanen, H., and Martikainen, P. J.: Seasonal variation in $CH_4$ emissions and production and oxidation potentials at microsites on an oligotrophic pine fen, Oecologia, 110, 414–422, 1997.
Schroeder, R., McDonald K. C., Champan, B.D., Jensen, K., Podest, E., Tessler, Z. D., Bohn, T. J., Zimmermann, R.: Development and evaluation of a multi-year fractional surface water data set derived from active/passive microwave remote sensing data, 7, 16688-16732, 2015.
Schütz, H., Seiler, W., Conrad, R.: Influence of soil-temperature on methane emission from rice paddy fields, Biogeochemistry, 11, 77–95, 1990.
Segers, R.: Methane production and methane consumption: a review of process underlying wetland methane fluxes, Biogeochemistry, 41, 23-51,1998.
Shannon, R. D. and White, J. R.: 3-Year Study of Controls on Methane Emissions from 2 Michigan Peatlands, Biogeochemistry, 27, 35–60, 1994.
Siavoshi., M., Dastan, S., Yassari, E., Laware, S. L.: Role of organic fertilizers on morphological and yield parameters in rice ( Oryza sativa L.), Intl. J. Agron. Plant Prod., 4, 1220-1225, 2013.
Sloan, V.: Plant roots in Arctic ecosystems: stocks and dynamics and their coupling to aboverground parameters*, PhD Thesis. University of Sheffield,* Sheffield, UK*,* 2011.
Smith, L. K., Lewis, W. M., Chanton, J. P., Cronin, G., and Hamilton, S. K.: Methane emissions from the Orinoco River floodplain, Venezuela, Biogeochemistry, 51, 113–140, 2000.
Song, C., Xu, X., Sun, X., Tian, H., Sun, L., Miao, Y., Wang, X., Guo, Y.: Large methane emission upon spring thaw from natural wetlands in the northern permafrost region, Environ. Res. Lett., 7, 034009, doi:10.1088/1748-9326/7/3/034009, 2012.
Starr, G., Oberbauer, S., Ahlquist, L.: The photosynthetic response of Alaskan tundra plants to increased season length and soil warming, Arct. Antarct. Alp. Res. 40(1), 181–191, 2008.
Sturtevant, C. S., Oechel, W. C., Zona, D., Kim, Y., and Emerson, C. E.: Soil moisture control over autumn season methane flux, arctic coastal plain of Alaska, Biogeosciences, 9, 1423–1440, 2012.

838 Sullivan, P. F., Welker, J. M.: Warming chambers stimulate early season growth of an
839 arctic sedge: results of a minirhizotron field study, Oecologia, 142, 616-626, 2005.
840 Svensson, B. H., Christensen, T. R., Johansson, E., and Oquist, M.:Interdecadal changes
841 in $CO_2$ and $CH_4$ fluxes of a subarctic mire:Stordalen revisited after 20 years, Oikos, 85,
842 22–30, 1999.
843 Tian, Y, Dickinson, R. E., Zhou, L., Zeng, X., Dai, Y., Myneni, R. B., Knyazikhin, Y.,
844 Zhang, X., Friedl, M., Yu, H., Wu, W., Shaikh, M.: Comparison of seasonal and
845 spatial variations of leaf area index and fraction of absorbed photosynthetically active
846 radiation from Moderate Resolution Imaging Spectroradiometer (MODIS) and
847 Common Land Model, J. Geophys. Res.,109, D01103, doi:10.1029/2003JD003777,
848 2004.
849 Tokida, T., Mizoguchi, M., Miyazaki, T., Kagemoto, A., Nagata, O., Hatano, R.:
850 Episodic release of methane bubbles from peatland during spring thaw, Chemosphere,
851 70, 165-171, 2007.
852 Torn, M. S., and Chapin III, F. S.: Environmental and biotic controls over methane flux
853 from arctic tundra, Atmos. Environ., 32, 3201–3218, 1993.
854 van Fischer, J. C., Rhew, R. C., Ames, G. M., Fosdick, B. K., von Fischer, P. E.:
855 Vegetation height and other controls of spatial variability in methane emissions from
856 the Arctic coastal tundra at Barrow, Alaska, J. Geophys. Res., 115, G00I03,
857 doi:10.1029/2009JG001283, 2010
858 van Hulzen J.B., Segers, R., van Bodegom, P. M., Leffelaar, P.A.: Temperature effects on
859 soil methane production: and explanation for observed variability, Soil Biol. and
860 Biochem., 31, 1919-1929, 1999.
861 van Winden, J. F., Reichart, G.-J., McNamara, N. P., Benthien, A., Damsté, J. S. S.:
862 Temperature-induced increase in methane release from peat bogs: a mesocosm
863 experiment, PLoS ONE 7(6): e39614. doi:10.1371/journal.pone.0039614, 2012.
864 Verma, A., Arkebauer, T. J., and Valentine, D.: BOREAS TF-11 $CO_2$ and $CH_4$ flux data
865 from the SSA-Fen. Data set, available at: http://www.daac.ornl.gov, Oak Ridge, TN,
866 USA, 1998.
867 Wang, C., Xiao, S., Li, Y., Zhong, H., Li, X., Peng, P.: Methane formation and
868 consumption processes in Xiangxi Bay of the Three Gorges Reservoir, Sci. Rep. 4,
869 444, doi:10.1038/srep04449, 2014.
870 Wania, R., Ross, I., and Prentice, I. C.: Implementation and evaluation of a new methane
871 model within a dynamic global vegetation model: LPJ-WHyMe v1.3.1, Geosci. Model
872 Dev., 3, 565–584, doi:10.5194/gmd-3-565-2010, 2010.
873 Wassmann, R., Thein, U. G., Whiticar, M. J., Rennenberg, H., Seiler,W., and Junk,W. J.:
874 Methane emissions from the Amazon floodplain: Characterization of production and
875 transport, Global Biogeochem. Cy., 6, 3–13, 1992.
876 Whalen, S. C., Reeburgh, W. S.: Consumption of atmospheric methane by tundra soils,
877 Nature, 342, 160–162, 1990.
878 Whalen, S. C. and Reeburgh,W. S.: Interannual variations in tundra methane emission: a
879 4-year time series at fixed sites., Global Biogeochem. Cy., 6, 139–159, 1992.
880 Whiting, G. J., Chanton, J. P.: Greenhouse carbon balance of wetlands: Methane
881 emission versus carbon sequestration, Tellus, 53B, 521-528, 2001.

882 Wickland, K. P., Striegl, R. G., Schmidt, S. K., Mast, M. A.: Methane flux in subalpine
883 wetland and unsaturated soils in the southern Rocky Mountains, Global Biogeochem.
884 Cycles, 13, 101–113, 1999.
885 Wilson, J. O., Crill, P. M., Bartlett, K. B., Sebacher, D. I., Harriss, R. C., Sass, R. L.:
886 Seasonal variation of methane emissions from a temperate swamp, Biogeochemistry,
887 8, 55-71, 1998.
888 Yvon-Durocher, G., Montoya, J. M., Woodward, G., Jones, J. I., Trimmer, M.: Warming
889 increases the proportion of primary production emitted as methane from freshwater
890 mesocosms, Global Chang. Biol., 17, 1225-1234, 2011.
891 Yvon-Durocher, G., Allen, A. P., Bastviken, D., Conrad, R., Gudasz, C., St-Pierre, A.,
892 Thanh-Duc, N., del Giorgio, P. A.: Methane fluxes show consistent temperature
893 dependence across microbial to ecosystem scale, Nature, 507, 488-491, 2014.
894 Zhuang, Q., Melillo, J. M., Kicklighter, D. W., Prinn, R. G., McGuire, A. D., Steudler, P.
895 A., Felzer, B. S., and Hu, S.: Methane fluxes between terrestrial ecosystems and the
896 atmosphere at northern high latitudes during the past century: A retrospective analysis
897 with a process based biogeochemistry model, Glob. Biogeochem. Cycles, 18,
898 GB3010, doi:3010.1029/2004GB002239, 2004.
899 Zona, D., Oechel, W. C., Kochendorfer, J., Paw U, Salyuk, A. N., Olivas, P. C.,
900 Oberbauer, S. F., Lipson, D. A.: Methane fluxes during the initiation of a large-scale
901 water table manipulation experiment in the Alaskan Arctic tundra, Global
902 Biogeochem. Cycle 23, GB2013, doi:10.1029/2009GB003487, 2009.
903 Zona, D., Gioli, B., Commane, R., Lindaas, J., Wofsy, S. C., Miller, C. E., Dinardo, S. J.,
904 Dengel, S., Sweeney, C., Karion, A., Chang, R.Y.-W., Henderson, J. M., Murphy, P.
905 C., Goodrich, J. P., Moreaux, V., Liljedahl, A., Watts, J. D., Kimball, J. S., Lipson, D.
906 A., Oechel, W. C.: Cold season emissions dominate the Arctic tundra methane budget,
907 PNAS, 113,40-45, 2016.

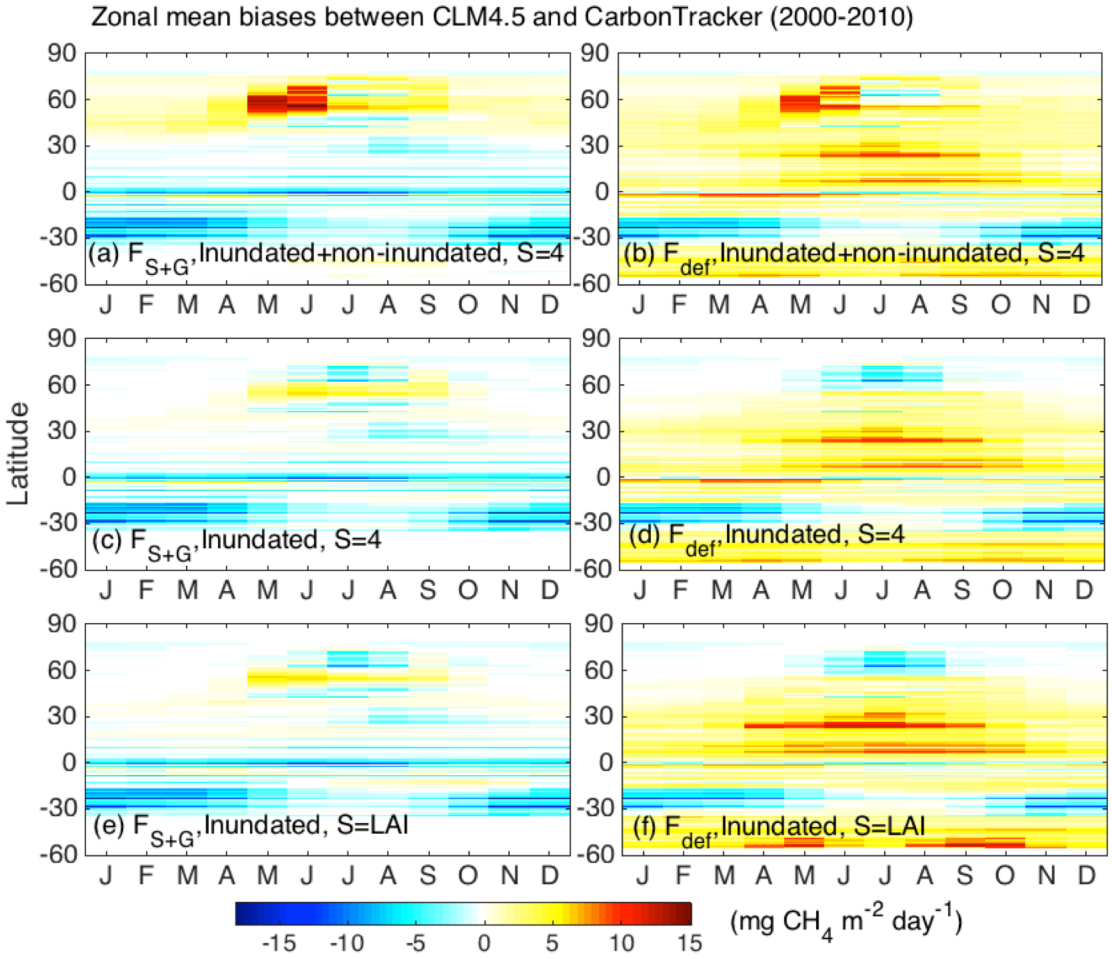


Fig. 1. Zonal mean biases of $CH_4$ emissions between CLM4.5 predictions and CarbonTracker ($CH_4$_CLM4.5-$CH_4$_CarbonTracker) with SWAMPS-GLWD ($F_{S+G}$) and CLM4.5 predicted ($F_{def}$) inundation fraction: CLM4.5 predictions of both inundated and noninundated emissions with $F_{S+G}$ (a) and $F_{def}$ (b), while aerechyma area is corrected with $S$=4; CLM4.5 predictions of inundated emissions only with $F_{S+G}$ (c) and $F_{def}$ (d), while aerechyma area is corrected with $S$=4; CLM4.5 predictions of inundated emissions only with $F_{S+G}$ (e) and $F_{def}$ (f), while aerechyma area is parameterized by default $S$=$LAI$.

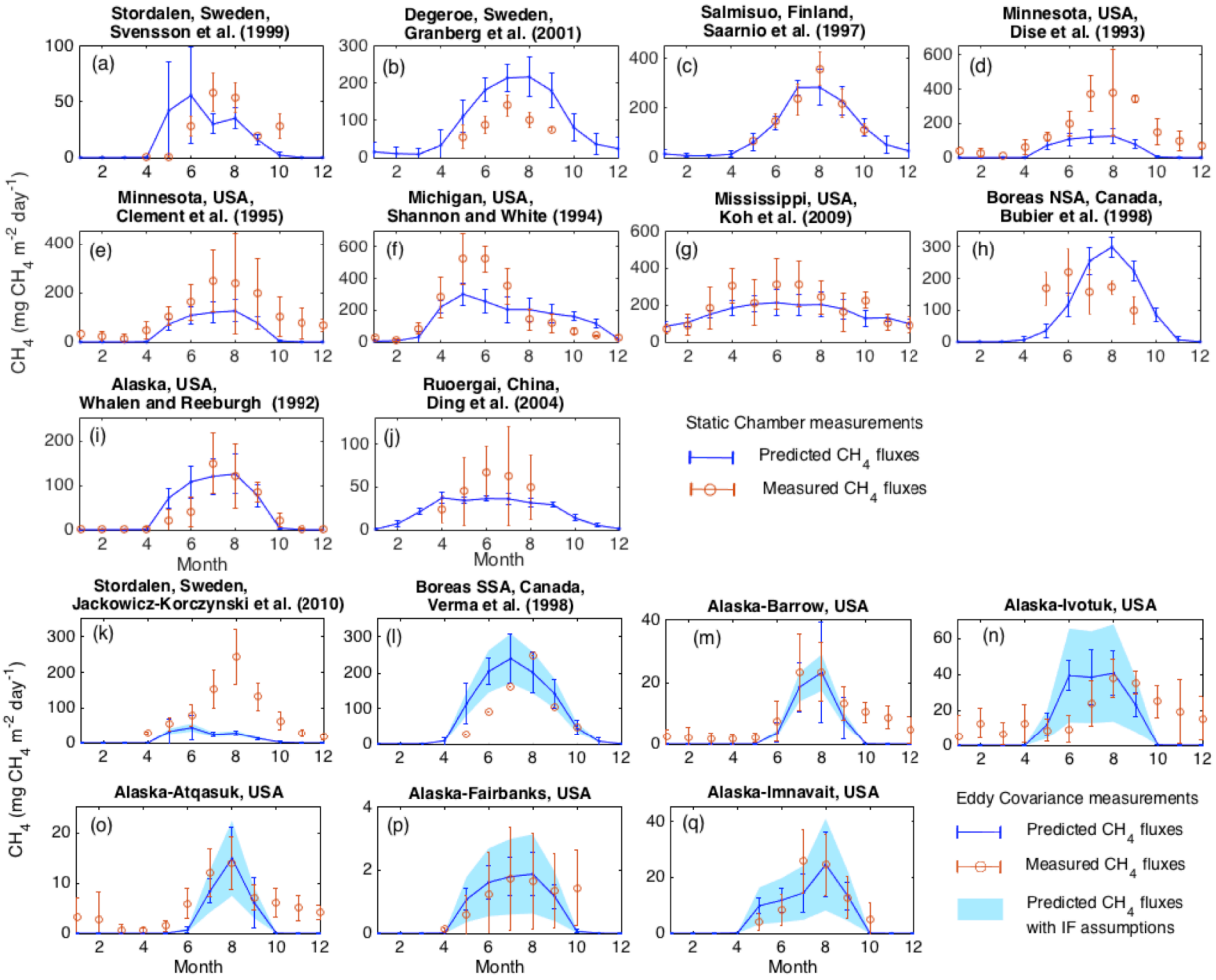


Fig. 2. Comparison of monthly mean simulated net $CH_4$ flux between 2000 and 2012 and observed monthly mean net $CH_4$ emissions in measurement year(s). The site measurements with static chamber are shown in (a-j) and measurements with eddy covariance (EC) towers are shown in (k-q). The error bars are standard deviation of monthly mean. The measurements with EC tower are weighted with a range of Inundation Fraction (IF) based on best estimates available: Stordalen: 80-100%; Boreas SSA: 50-90%; Alaska-Barrow: 60-100%, Alaska-Atqasuk: 10-30%; Alaska-Ivotuk: 5-25%; Alaska-Fairbanks:0.5-2.5%, Alaska-IMN:5-25%. Detailed description of the sites and measurements are shown in Table S1.

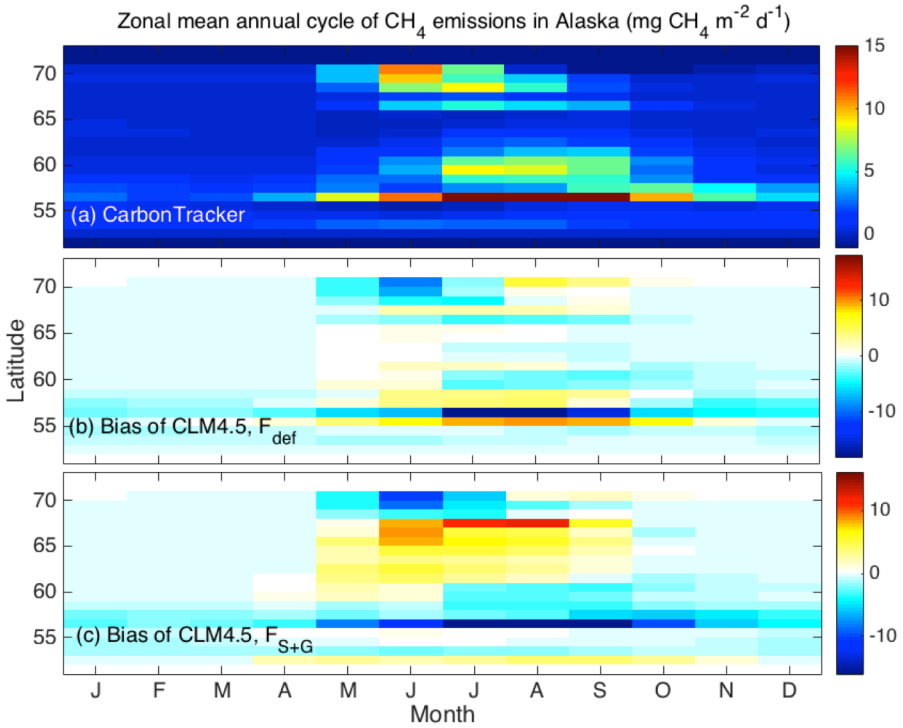


Fig. 3. The 2000-2010 zonal mean annual cycle of $CH_4$ emission (mg $CH_4$ $m^{-2}$ $day^{-1}$) across Alaska predicted by CarbonTracker (a), and biases of CLM4.5 with CLM4.5 predicted inundation fraction ($F_{def}$) (b) and SWAMPS-GLWD inundation fraction ($F_{S+G}$) (c). The 0.5°×0.5° CLM4.5 is regridded to 1°×1° to be consistent with CarbonTracker.

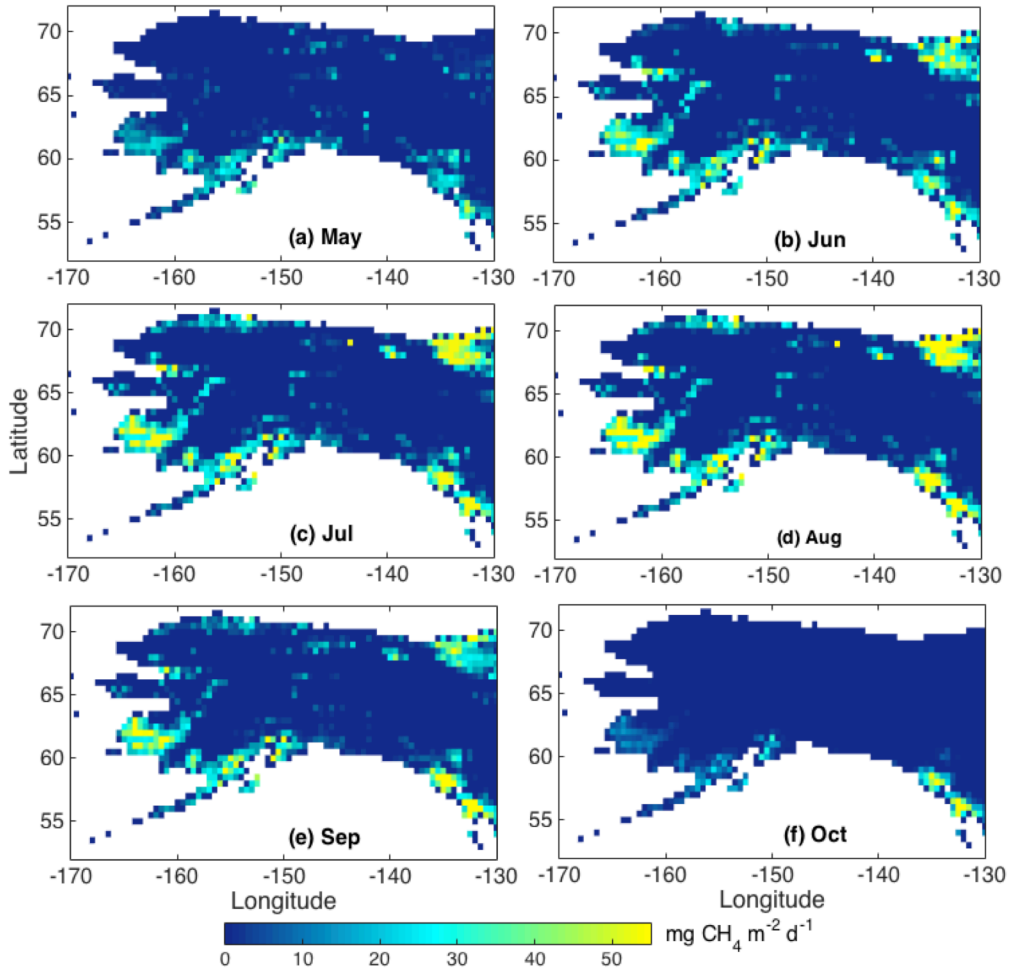


Fig. 4. CLM4.5 simulated mean monthly $CH_4$ emissions with $F_{def}$ across years 2000-2012.

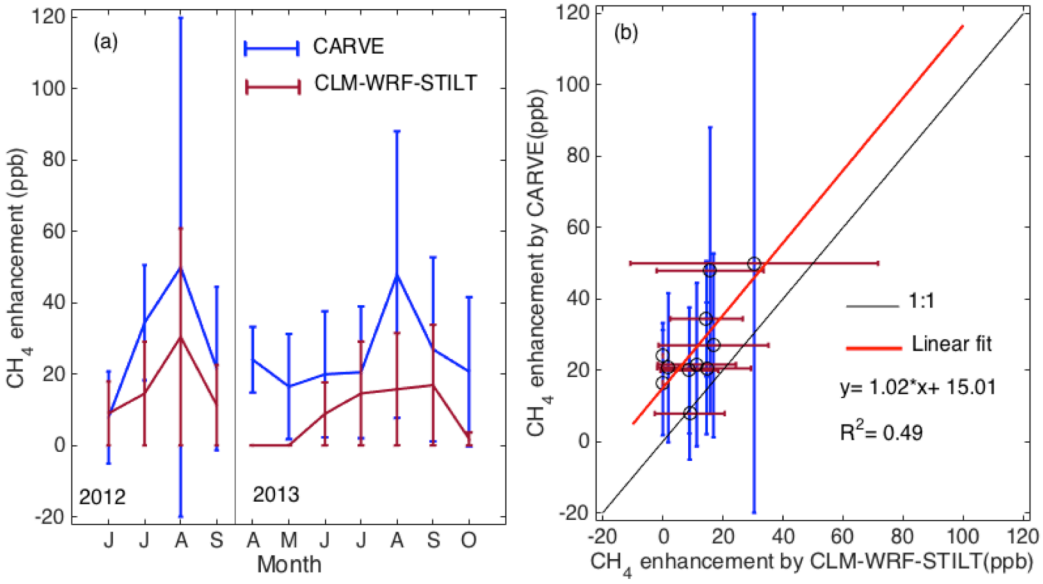


Fig. 5. The monthly mean atmospheric mole fraction enhancements in $CH_4$ estimated by WRF-STILT-CLM4.5 and CARVE measurements. (a) Observed and simulated monthly $CH_4$ mole fraction enhancements in 2012 and 2013; (b) Linear regression of measured versus modeled $CH_4$ mole fraction enhancements. The error bars are standard deviation of monthly mean.

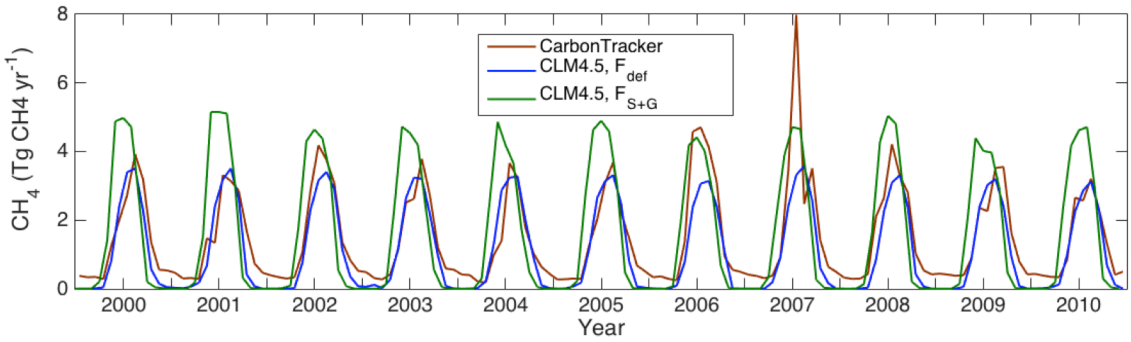


Fig. 6. Time variation of integrated $CH_4$ (Tg $CH_4$ $yr^{-1}$) emissions from Alaska by CarbonTracker (brown), CLM4.5 with internally-predicted fraction of inundation $F_{def}$ (blue) and CLM4.5 SWAMPS-GLWD fraction of inundation $F_{S+G}$ (green).

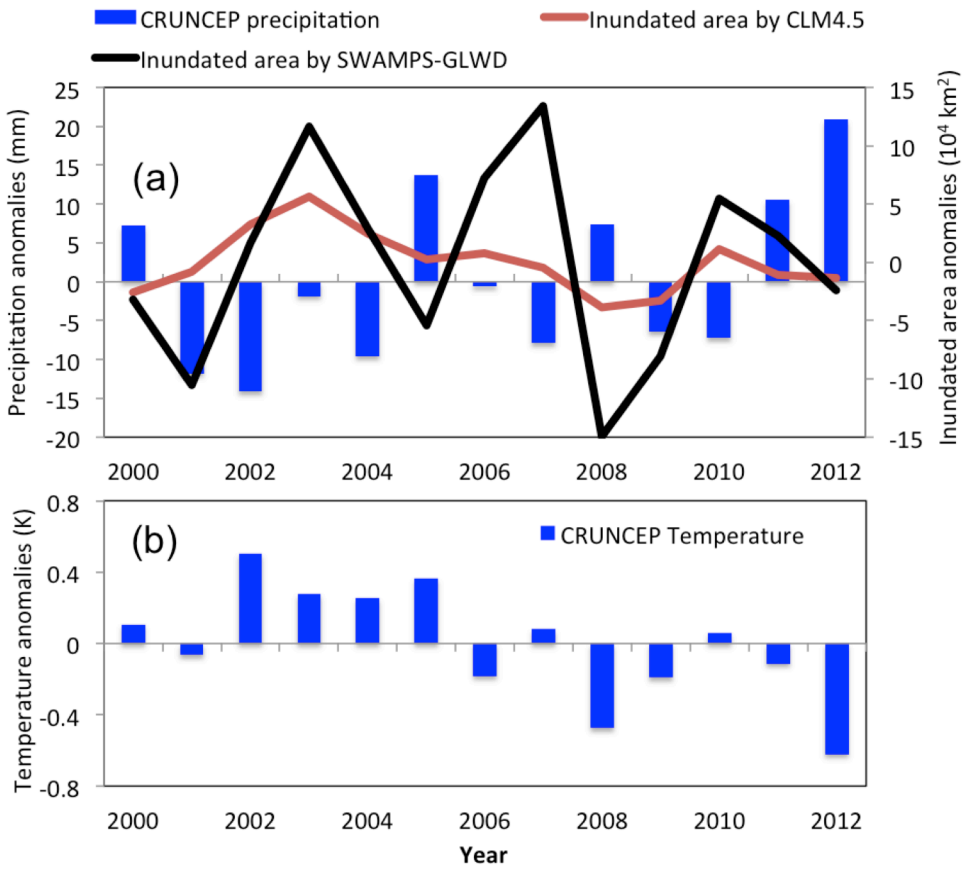


Fig. 7. The anomalies of annual precipitation and inundated area in Alaska (a) and the anomalies of annual mean temperature (b). The anomalies are calculated by subtracting the average between 2000-2012.

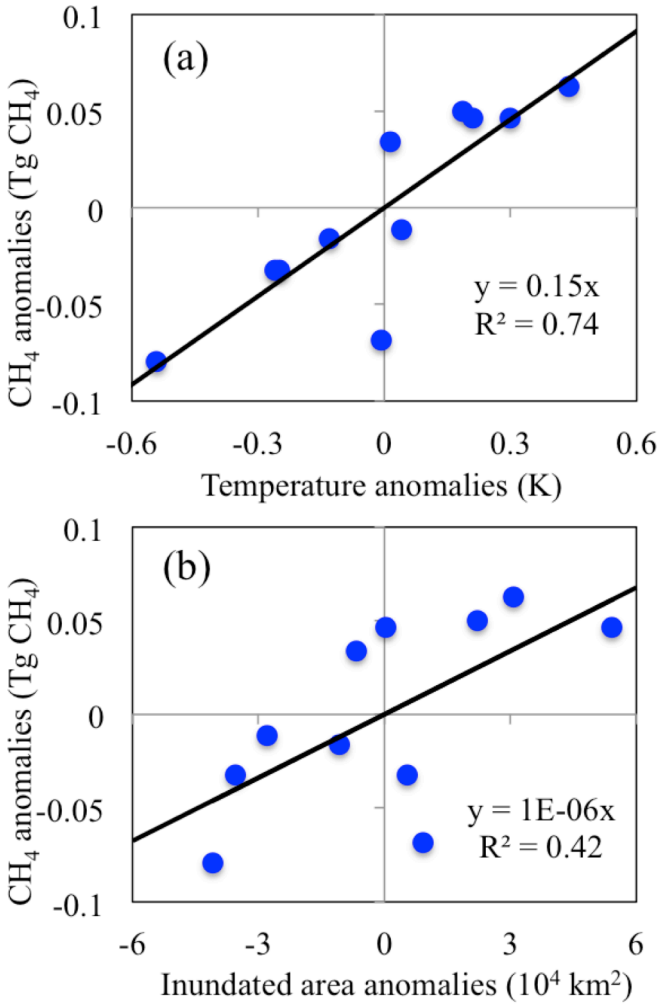


Fig. 8. The correlation between CLM-predicted annual $CH_4$ emission anomalies and mean annual temperature anomalies (a) and correlation between annual $CH_4$ emission anomalies and predicted inundated area anomalies during 2000-2010. The anomalies are calculated by subtracting the average between 2000-2010.